*Conference on Modelling Fluid Flow (CMFF'25)*
*The 19th International Conference on Fluid Flow Technologies*
*Budapest, Hungary, August 26 -August 29, 2025*

# LAMINAR – TURBULENT TRANSITION IN HELICALLY COILED REACTORS. AN EXPERIMENTAL STUDY WITH HIGH-SPEED PIV

C. Müller[1*], P. Kováts[1], D. Thévenin[1], K. Zähringer[1]

[1] Laboratory of Fluid Dynamics and Technical Flows, Otto-von-Guericke-Universität Magdeburg. Universitätsplatz 2, D-39106 Magdeburg, Germany. Tel.: +49 391 - 67 58654, Fax: +49 391 - 67 52840
*E-mail: conrad.mueller@ovgu.de

## ABSTRACT

Helically coiled reactors (HCRs) are widely used in process engineering and biochemistry, especially in micro-reactor applications, to enhance heat and mass transfer. Their design promotes excellent radial mixing with minimal axial back-mixing. At moderate Reynolds numbers, characteristic Dean vortices form within HCRs. Increasing flow velocities lead to more complex vortex structures. The transition from laminar to turbulent flow significantly impacts reactor performance.

Various experimental and numerical studies have attempted to characterize this transition, often using a critical Reynolds number based on the curvature ratio δ = d/D. Although it is generally accepted that HCRs have higher critical Reynolds numbers than straight tubes, reported values differ widely, possibly due to variations in experimental setups and inlet conditions.

We propose a novel experimental setup designed to minimize the influence of inlet and outlet conditions. Reynolds numbers from 460 to 9,650 were examined. Initial Laser Doppler Anemometry (LDA) measurements reveal that velocity fluctuations are weaker near the inner wall and stronger near the outer wall. High-speed Particle Image Velocimetry (PIV) measurements corroborate these findings. Additionally, we demonstrate how inlet conditions influence the transition point and introduce different markers for the laminar-turbulent transition in HCRs through pseudo-3D visualizations, frequency analysis, and qualitative flow analysis.

**Keywords: Helically coiled reactor, PIV, spectral entropy, transition, turbulence**

## NOMENCLATURE

| | | |
|---|---|---|
| $d$ | [mm] | inner tube diameter |
| $D$ | [mm] | coil diameter |
| $\delta = d/D$ | [-] | curvature ratio |
| $\eta$ | $[\frac{kg}{ms}]$ | dyn. viscosity |
| $\rho$ | [kg/m³] | density |
| $Q$ | [-] | Q-criterion |
| $\dot{V}$ | [l/min] | volume flow rate |
| $u_r$ | [m/s] | radial velocity |
| $u_a$ | [m/s] | axial velocity |
| $f$ | [$s^{-1}$] | frequency |
| $f_{rec}$ | [$s^{-1}$] | recording frequency |
| $Re = \rho u d/\eta$ | [-] | Reynolds number |
| FEP | Fluorethylenepropylene | |
| LDA | Laser Doppler Anemometry | |
| PIV | Particle Image Velocimetry | |
| PMMA | Polymethylmethacrylate | |

## 1. INTRODUCTION

The laminar-turbulent transition in helically coiled reactors is widely researched with different approaches since first studies done by Taylor [1] and White [2] in 1927. Figure 1 shows the most important literature findings regarding the transition in HCRs.

The black curves represent studies measuring the pressure drop over HCRs or curved tubes, where the transition is marked by the critical Reynolds number in function of the curvature ratio δ = d/D being the ratio of the inner diameter of the tube and to coiling diameter [3-7]. The red curves represent studies measuring the velocity field in the HCRs by using hot wire anemometry [8], LDA or (stereo-) PIV [9, 10]. The transition in those studies is determined by the velocity fluctuations in function of time with a threshold or qualitative analysis. More modern approaches use the frequency spectrum or energy dissipation rate. Outstanding here is the work of Sreenivasan and Strykowski [8] suggesting a transition region with a low Reynolds number for a first occurrence of fluctuations and a higher boundary where the flow becomes completely turbulent in the whole cross-section of the reactor tube.

As Figure 1 represents, the transition point to turbulence in HCRs is a broad range. The differences between researchers lay in different measurement

techniques and the definition of a turbulent flow itself. Recent numerical studies [11, 12] promote the lower boundary for the transition.

However, all of those studies lack a detailed visualization of the flow structures in the whole tube, often just using single points in the reactors for the analysis. These can most definitely mark a certain state of turbulence, but not the full behaviour of the transition process in HCRs with its more complex vortex structures like Lyne vortices [13] and the geometrical differences of their appearance. Moreover, the deformed pipe flow in HCRs caused by the radial forces leads to an asymmetric problem that seems to be overlooked.

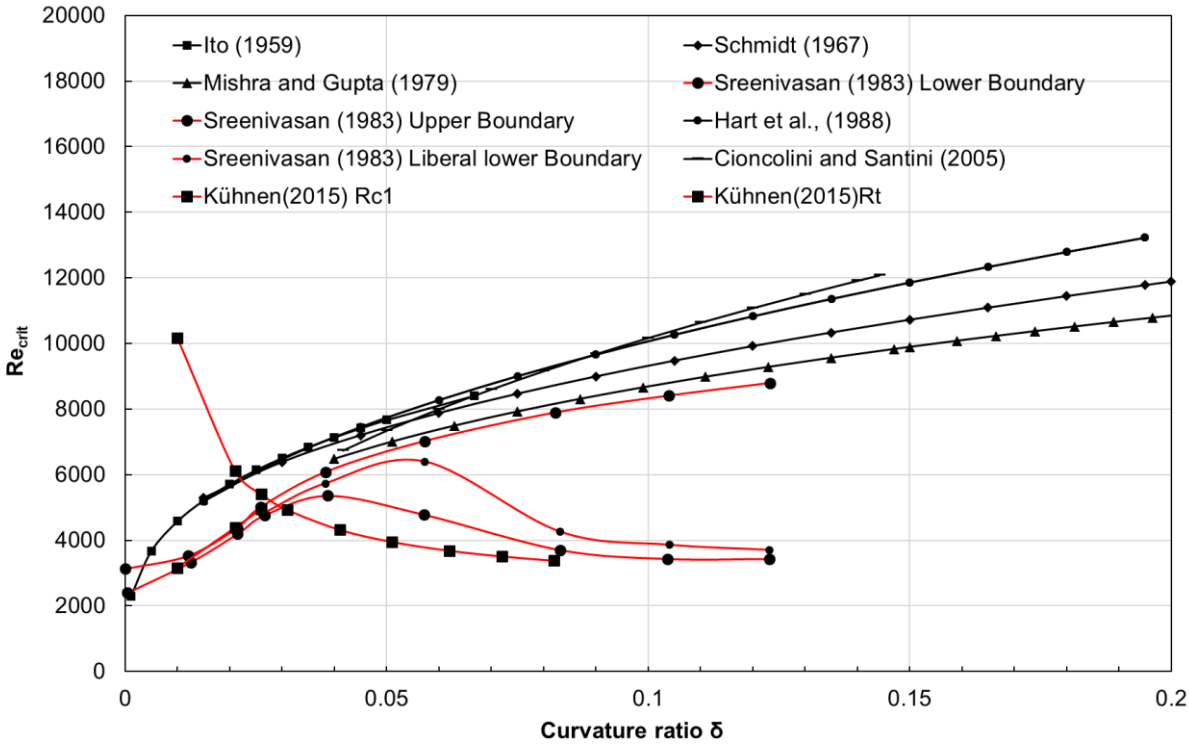


**Figure 1. Laminar-turbulent transition in HCRs from literature marked by the critical Reynolds number in function of the curvature ratio δ = d/D.**

This work establishes a measuring setup with a very high temporal and spatial resolution, paired with modern visualization approaches and analysis aiming for a highly resulted data base which is used to clarify the transition behaviour and pinpoint the actual transition point. Therefore, the measured Reynolds numbers cover the whole range of possible transitions as suggested by literature (Figure 1).

## 2. EXPERIMENTAL SETUP

The helix reactor is made of FEP-tube with an inner diameter of 10 mm and a coil diameter of 118 mm resulting in a curvature ratio of δ=0.0848. In total 50 coils are realized resulting in a tube length of 18.53 metres with additional one metre straight inlet and outlet tube. For the high speed PIV setup, the HCR is placed in an acrylic glass tank filled with a 5.25%vol. Glycerol and de-ionised water solution, which is also used as the working fluid. The solution matches the refractive index of the FEP tube (n = 1.3405) [14]. The solution has a density of 1004.045 kg/m³ and a dynamic viscosity of 0.001246 kg $m^{-1}$ $s^{-1}$ (measured with Netzsch Kinexus Pro+). Vestosint PMMA particles with 50 µm diameter are added to the working fluid as tracer particles.

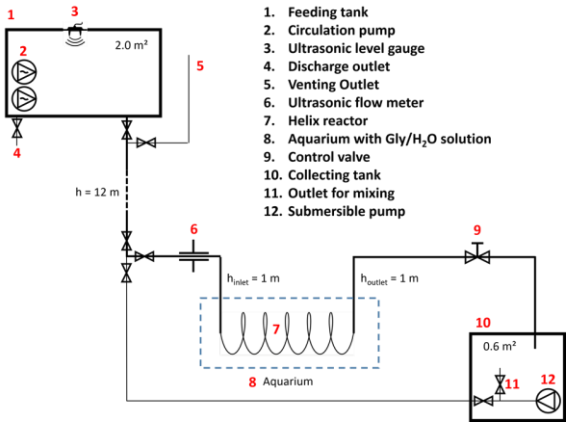


**Figure 2. Flow sketch of the experimental setup.**

A feeding tank is placed 12 m above the main setup creating a completely gravity driven and so pulsation free flow (Figure 2). The flow rate is measured with an ultrasonic flow metre and controlled with a needle valve at the outlet. Since the

measurements are run as a batch process and the flow rate has to stay stable, the level in the feeding tank has been controlled with a ultrasonic level sensor and a pressure level sensor.

A Phantom VEO L640 high-speed camera (2560x1600 pixels) is set in front of the tank with a 100 mm camera lens (Tokina, AT-X Pro Macro 100 F2.8D) to face the tank as shown in Figure 3 below.

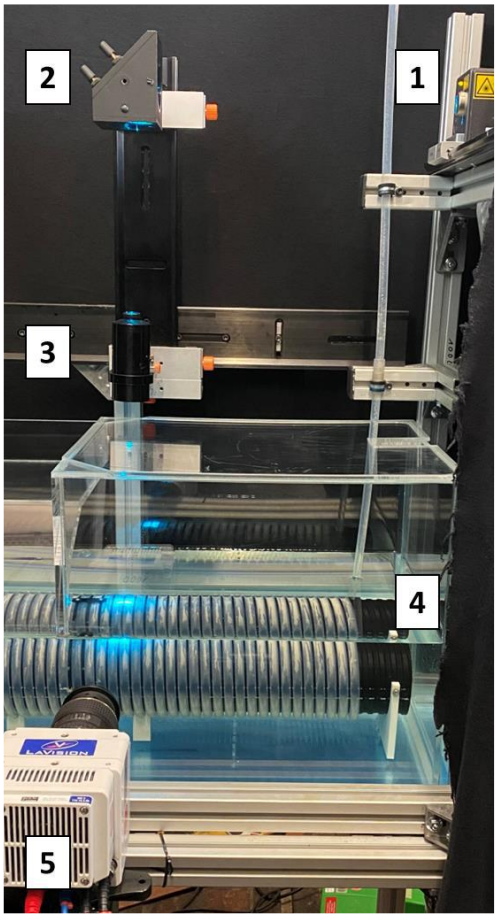


**Figure 3. Optical high-speed PIV setup of the cw-laser (1), mirror (2), light sheet optics (3), aquarium with refractive index matched solution, helix reactor (4) and HS-camera (5).**

The light source is a continuous-wave laser from Coherent (Model: Genesis MX488-1000 STM) with 488 nm wavelength operated at 120 mW power. The geometrical calibration results in a ~55 pixel/mm resolution. For selected Reynolds numbers in a range of 460 < Re < 9650, flow rates are set and the pixel shift is kept around 2 pixels between snapshots. The relatively small pixel shift is necessary due to the strong out-of-plane movement, since the axial velocity is 10 times higher compared to the radial velocities. For all measurements at least 2 seconds are recorded with different recording frequencies depending on the Reynolds number and listed in Table 1. Also, the axial velocity was measured with PIV, by measuring in the front section of the coil. The light sheet was therefore set in the centre of the tube and the camera was adjusted accordingly. Figure 4 shows a sketch of the setups for the radial measurements in the cross-section of the tube and for the axial measurements in the centre of the front of the coil.

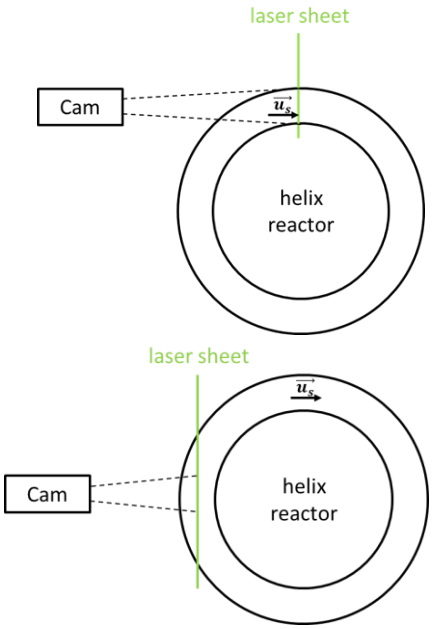


**Figure 4. Sketch of the PIV set-ups. Top: radial velocity components. Bottom: axial component is measured in the centre of the tube.**

The images are then processed with DaVis 10.2 (LaVision) and visualized with ParaView 5.10.

All measurements are taken at the 40$^{th}$ coil of the HCR where the influence of inlet and outlet vanish. This was proven in previous tests with LDA measurements [15] and will also be validated here with the axial PIV measurements (see Figure 6).

**Table 1. Recording parameters of radial and axial PIV measurements**

| | | Radial | Axial |
|---|---|---|---|
| $Re$ | $\dot{V}$ | $f_{rec}$ | $f_{rec}$ |
| $[-]$ | $[l/min]$ | $[kHz]$ | $[kHz]$ |
| 460 | 0.27 | 0.4 | 1.0 |
| 920 | 0.54 | 0.6 | 2.0 |
| 1370 | 0.80 | 0.8 | 3.0 |
| 2100 | 1.23 | 1.1 | 4.6 |
| 2750 | 1.61 | 1.4 | 6.0 |
| 3660 | 2.14 | 1.8 | 8.0 |
| 4580 | 2.68 | 2.2 | 10.0 |
| 5510 | 3.22 | 2.6 | 12.0 |
| 6410 | 3.75 | 3.0 | 12.0 |
| 7340 | 4.29 | 3.4 | 12.0 |
| 8240 | 4.82 | 3.8 | 12.0 |
| 9170 | 5.36 | 4.2 | 12.0 |
| 9650 | 5.64 | 4.5 | 12.0 |

## 3. POSTPROCESSING

The postprocessing is done in DaVis and consists of an image calibration, a subtraction of a median Gauss filter to enhance the particle images and the PIV processing followed by a vector postprocessing step as clean-up of erroneous vectors. The resulting vector fields are further treated to identify the transition point to turbulence.

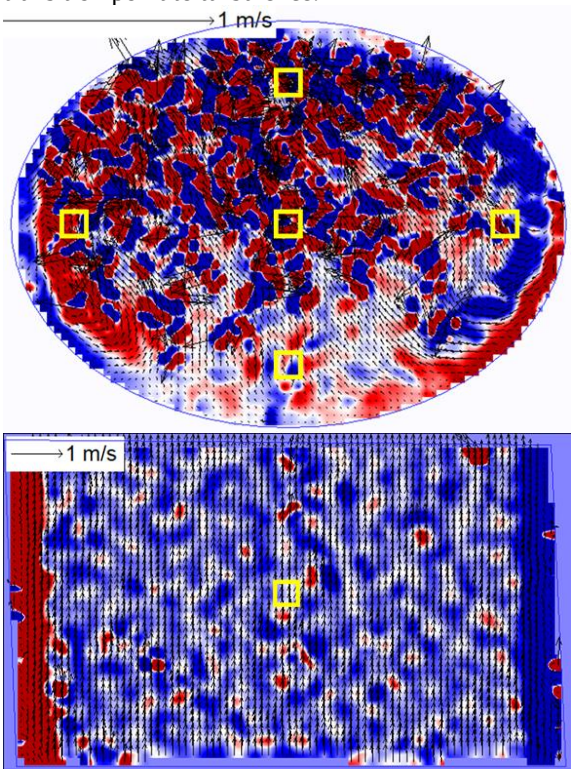


**Figure 5. Instantaneous flow fields of the radial velocity (top) and the axial velocity (bottom) with the extraction points of the velocity over time marked in yellow.**

First, the local velocity is extracted at 5 points in the cross-section, marked with yellow boxes in Figure 5, and plotted in function of time (Figure 7). In addition, the centre velocity from the axial velocity field (Figure 5 bottom) is extracted and plotted over time to visualise the fluctuations (Figure 8).

Second, the frequency spectrum is analysed from the axial velocity over time plots using FFT (Table 2 and Figure 10).

Third, pseudo-3D vortex structures are reconstructed (Figure 11) from the vector fields. Therefore, the vector fields of the tube cross-section (radial velocity) are stacked in a third plane representing time. This third axis is normalized by dividing the superficial velocity with the recording frequency resulting in the third dimension being in metres. A detailed description of those pseudo 3D-visualizations is found in Müller, Kováts [16]. From these 3D-fields vortices are represented with the Q-Criterion as isosurface coloured by the Z-vorticity for a qualitative analysis.

## 4. RESULTS

In order to test the independency of the measurement position from the inlet and outlet conditions, the axial velocity was measured in each coil. It is then extracted as velocity over time plot at the centre position (yellow square in Figure 5 bottom image) and its standard deviation normalized by the average velocity is plotted in function of the coil number in Figure 6.

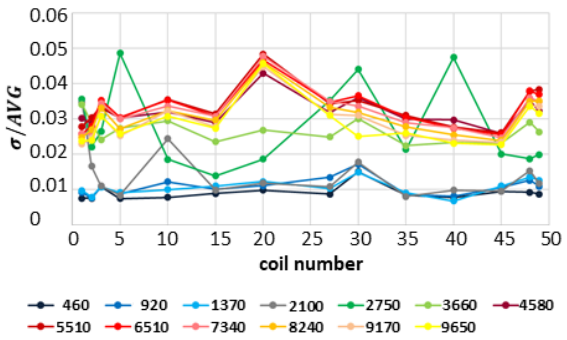


**Figure 6. Normalized standard deviation of all Reynolds numbers in function of the coil number.**

After the first 3 coils where the initial straight tube flow gets forced into the radial flow structure the standard deviation stabilizes due to the re-laminarizing effects of the coiled flow. However, only after 30-40 coils a full stabilization is realized. Especially at moderate Reynolds numbers (Re = 2100, 2750, 3660) the flow needs at least 30 coils to stabilize. Also noticeable is the impact of the outlet with a sudden increase of the standard deviation for the last 2 coils.

The normalized standard deviation (also known as turbulence intensity) of the axial velocities sorts itself into two regions. Low Reynolds numbers up to Re = 2200 have a σ/AVG of 0.01. Reynolds numbers higher than Re = 3830 have a σ/AVG value of 0.03 to 0.04, so four times higher. Kühnen, Braunshier [9] described that increase in standard deviation also as indicator for the laminar turbulent transition. A transition area can be noticed for Reynolds numbers between $2200 < Re < 3830$ where the curves do not fit to the above mentioned groups.

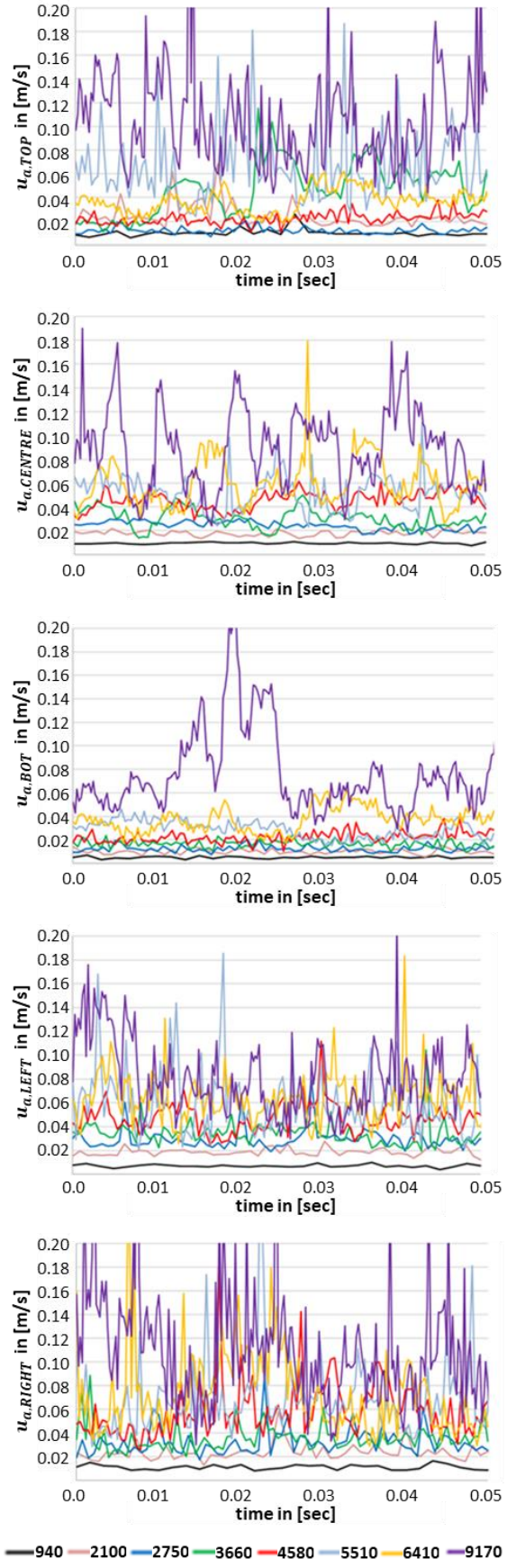


**Figure 7. Extracted radial velocity over time of different Reynolds numbers. Locations from top to bottom: Top, Centre, Bottom, Left, Right.**

Figure 7 above shows the velocity in function of time from the 5 points shown in Figure 5. From these plots it is obvious, that with rising Reynolds number the fluctuations of the flow become stronger, there are also clear differences depending on the location in the cross-section of the coil. While the fluctuations start to become strong at Re = 4500 in the top, as well as left and right where the Dean vortices are situated, they are much less pronounced in the centre and almost neglectable in the bottom.

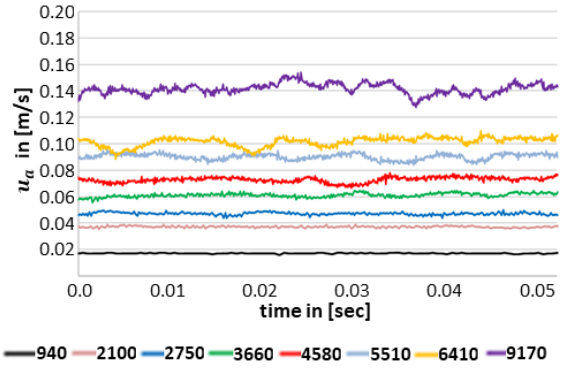


**Figure 8. Extracted axial velocity over time of different Reynolds numbers.**

The axial velocities over time in Figure 8 have a similar trend with an increase of fluctuations with rising Reynolds number. When taking a look onto a full measurement period (Figure 9) not only high frequency fluctuations but also oscillation waves with lower frequencies become visible.

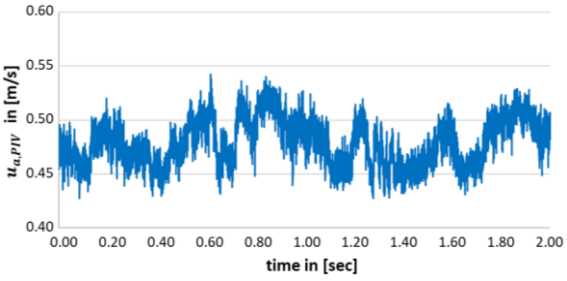


**Figure 9. Extracted axial velocity over time of Reynolds number 2880 for the whole measurement time of 2 seconds.**

The following Figure 10 shows the frequency spectra of some Reynolds numbers for the axial measurements. As expected, in a completely laminar flow (Re=480) no frequencies could be detected. At medium Reynolds numbers some frequencies are more pronounced. With rising Reynolds number, the frequency spectrum broadens until no frequencies stand out anymore. The two highest detected frequencies are listed in Table 2 below.

**Table 2. Highest detected frequencies from FFT for selected Reynolds numbers.**

| Re | $f_1$ | $f_2$ |
|---|---|---|
| 460 | - | - |
| 2750 | 1 Hz | 3 Hz |
| 3660 | 6 Hz | 36 Hz |
| 5510 | 7 Hz | 22 Hz |
| 9650 | Spectrum | |

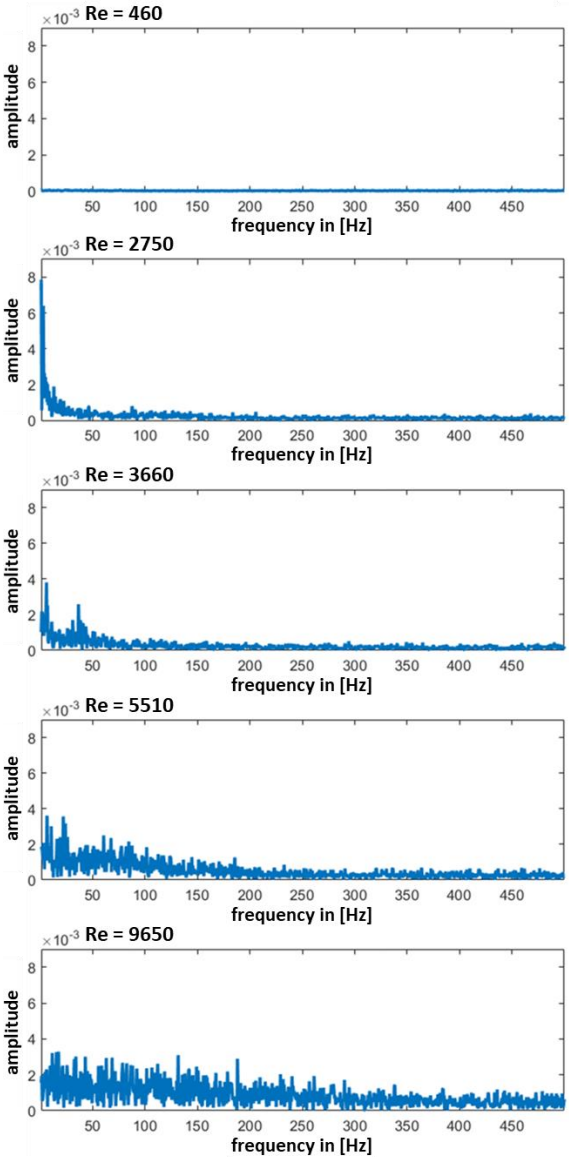


**Figure 10. Frequency spectra of selected Reynolds numbers from the FFT analysis of extracted axial velocities.**

For a more detailed analysis of the flow it seemed reasonable to visualize the flow as a whole. The instantaneous flow fields are therefore extended to pseudo-3D-visualizations. Figure 11 below shows a selection of Reynolds numbers in an unrolled top-down view of the helix tube. The flow goes from left to right, visualized is the vortex occurrence by the Q-Criterion, coloured with the Z-Vorticity. The represented pseudo distance of 100 mm contains around 500 images depending on the recording frequency and superficial velocity. At low Reynolds number the counter rotating Dean vortices are clearly visible as horizontal stripes near the tube walls indicating a stable and laminar flow. With increasing Reynolds number, Lyne vortices near the centre of the cross-section occur. They merge with the Dean vortices on either side and finally disappear, indicating first instabilities and transition to turbulence (Figure 11, Re = 2750). With even faster flows the Lyne vortices appear with higher frequency and are more unstable (Re=3660). At a certain point the Lyne vortices are no longer distinguishable and the whole flow becomes turbulent. Even the Dean vortices become smeared indicating a completely turbulent flow behaviour (Figure 11, Re = 5510). At the highest measured flow rate with a Reynolds number of Re = 9650, the additional vortex structures have even the same intensity and size as the Dean vortices. It has to be noted, that with increasing Reynolds number the overall vorticity also rises steadily.

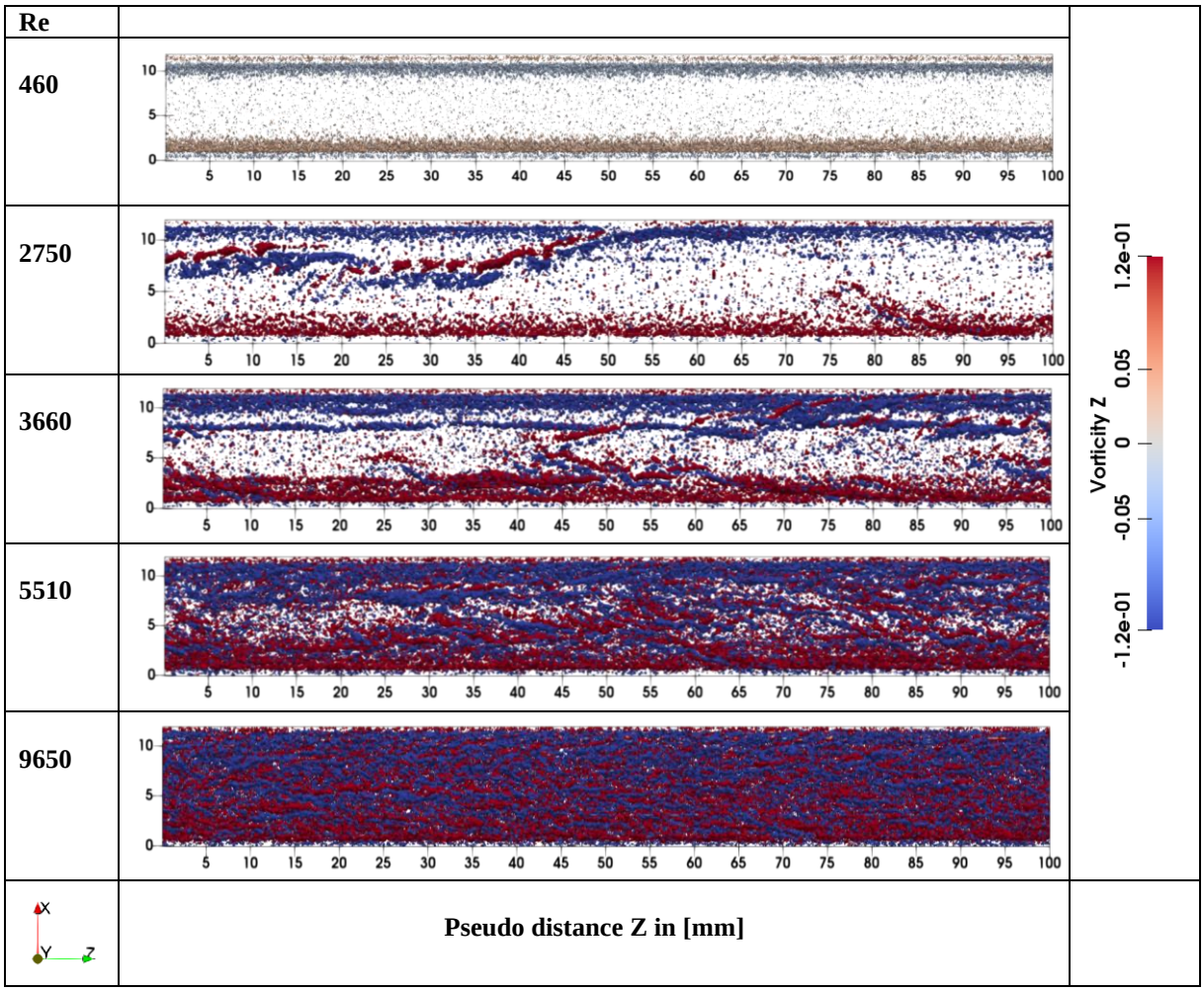


**Figure 11. Pseudo-3D-visualizations of the radial velocity fields. Q = 0.0035 to 0.05; Z-Vorticity = - 0.125 to 0.125 (for Re = 460; Q = 0.00035 to 0.05).**

## 5. CONCLUSIONS

In this study, the laminar-turbulent transition of helical coils is examined by LDA and PIV measurements. The independence of inlet and outlet conditions was proven for the set-up with a HCR of 50 coils in a range of coil numbers 30 to 40.

The qualitative analysis of the velocities, measured in the 40$^{th}$ coil, confirms the findings of Sreenivasan and Strykowski [8]. Depending on the location in the cross-section of the helix the flow behaves differently. While in the outer region of the HCR, or here in the top of the cross-section, fluctuations indicate turbulence at lower Reynolds numbers (Re = 5700), the turbulent behaviour in the inner region, here the bottom of the cross-section, is only pronounced at the highest measured Reynolds number of Re = 9650.

The FFT analysis of the axial velocities did not show detectable frequencies for laminar flow conditions. In the transition area some characteristic frequency peaks appear, and a broadening of the frequency spectrum in the completely turbulent region can be recognized.

The pseudo-3D-visualizations of the radial velocities showed the first instabilities as Lyne vortices at Reynolds number Re = 2750 and a fully turbulent flow behaviour at Re = 5510.

## OUTLOOK

While searching for the laminar-turbulent transition point in HCRs it becomes clear, that in the asymmetric flow a high dependency on the location is given. The here presented markers for the transition point are either focused on one point in the flow or are just of qualitative nature. For quantitative analysis, measurements of high spatial and temporal resolution are necessary to capture the occurring vortex structures with low experimental noise. A multitude of markers can help to capture all flavours of turbulence making a difference between stable or frequent structures like Lyne vortices and fully turbulent flow with a high vortex dissipation rate. A holistic view of all markers is necessary as validation but also to make a final decision on the transition point.

## ACKNOWLEDGMENTS

Funded by the Deutsche Forschungsgemeinschaft (DFG, German Research Foundation) – 444994527. The authors would like to thank their student Justus Herzig for his help and support with carrying out the measurements.

## REFERENCES

1. Taylor, G.I., *The criterion for turbulence in curved pipes.* Royal Society Publishing, 1927.
2. White, C.M., *Streamline flow through curved pipes.* Proceedings of the Royal Society of London. Series A, Containing Papers of a Mathematical and Physical Character, 1927. **123**(792): p. 645-663.
3. Itó, H., *Friction Factors for Turbulent Flow in Curved Pipes.* Journal of Basic Engineering, 1959: p. 123-132.
4. Schmidt, E.F., *Warmeubergang und Druckverlust in Rohrschlangen.* Zeitschrift fur Technische Chemie, Verfahrenstechnik und Apparatewesen, 1967. **39**: p. 781-832.
5. Mishra, P. and S.N. Gupta, *Momentum Transfer in Curved Pipes 1. Newtonian Fluids.* Ind. Eng. Chern. Process Des. Dev., 1978. **18**.
6. Hart, J., J. Ellenberger, and P.J. Hamersma, *Single and Two Phase Flow through helically coiled tubes.* Chemical Engineering Science, 1988. **43**: p. 775-783.
7. Cioncolini, A. and L. Santini, *An experimental investigation regarding the laminar to turbulent flow transition in helically coiled pipes.* Experimental Thermal and Fluid Science, 2006. **30**(4): p. 367-380.
8. Sreenivasan, K.R. and P.J. Strykowski, *Stabilization effects in flow through helically coiled pipes.* Experiments in Fluids, 1983. **1**: p. 31-36.
9. Kühnen, J., et al., *Subcritical versus supercritical transition to turbulence in curved pipes.* Journal of Fluid Mechanics, 2015. **770**.
10. Kühnen, J., et al., *Experimental investigation of transitional flow in a toroidal pipe.* Journal of Fluid Mechanics, 2013. **738**: p. 463-491.
11. Gelfgat, A.Y., *A comparative study on instability of steady flows in helical pipes.* Fluid Dynamics Research, 2020. **52**(1).
12. Canton, J., P. Schlatter, and R. Örlü, *Modal instability of the flow in a toroidal pipe.* Journal of Fluid Mechanics, 2016. **792**: p. 894-909.
13. Müller, C., P. Kováts, and K. Zähringer, *On the existence, formation and stabilization of Lyne vortices in helically coiled reactors at moderate Reynolds numbers*, in *20th International Symposium on the Application of Laser and Imaging Techniques to Fluid Mechanics, Lissabon, Portugal*. 2022.
14. Kováts, P., et al., *Mixing characterization in different helically coiled configurations by laser-induced fluorescence.* Experiments in Fluids, 2020. **61**(9).
15. Müller, C., P. Kováts, and K. Zähringer, *Experimental investigation of the laminar-turbulent transition in helically coiled reactors with LDA*, in *Fachtagung "Experimentelle Strömungsmechanik" GALA, München, Deutschland*. 2023.
16. Müller, C., P. Kováts, and K. Zähringer, *Experimental characterization of mixing and flow field in the liquid plugs of gas–liquid flow in a helically coiled reactor.* Experiments in Fluids, 2021. **62**(9).